The geometric effect and programming current reduction in cylindrical-shaped phase change memory

2009 Nanotechnology 20 285701

(http://iopscience.iop.org/0957-4484/20/28/285701)

Nanotechnology **20** (2009) 285701 (7pp) doi:10.1088/0957-4484/20/28/285701

The geometric effect and programming current reduction in cylindrical-shaped phase change memory

Yiming Li[1,2], **Chih-Hong Hwang**[1], **Tien-Yeh Li**[1] **and Hui-Wen Cheng**[1]

[1] Department of Electrical Engineering, National Chiao-Tung University, Hsinchu 300, Taiwan
[2] National Nano Device Laboratories, Hsinchu 300, Taiwan

E-mail: ymli@faculty.nctu.edu.tw

Received 30 March 2009, in final form 27 May 2009
Published 24 June 2009
Online at stacks.iop.org/Nano/20/285701

Abstract

This study conducts a three-dimensional electro-thermal time-domain simulation for numerical analysis of cylindrical-shaped phase change memories (PCMs). The influence of chalcogenide material, germanium antimony telluride (GeSbTe or GST), structure on PCM operation is explored. GST with vertical structure exhibits promising characteristics. The bottom electrode contact (BEC) is advanced to improve the operation of PCMs, where a 25% reduction of the required programming current is achieved at a cost of 26% reduced resistance ratio. The position of the BEC is then shifted to further improve the performance of PCMs. The required programming current is reduced by a factor of 11, where the resistance ratio is only decreased by 6.9%. However, the PCMs with a larger shift of BEC are sensitive to process variation. To design PCMs with less than 10% programming current variation, PCMs with shifted BEC, where the shifted distance is equal to 1.5 times the BEC's radius, is worth considering. This study quantitatively estimates the structure effect on the phase transition of PCMs and physically provides an insight into the design and technology of PCMs.

(Some figures in this article are in colour only in the electronic version)

1. Introduction

Phase change memories (PCMs) [1–7] are promising in solid-state memory technologies due to their high resistance contrast, good endurance, high-speed and low-voltage operation [8, 9], and well matched Si processes and complementary metal oxide semiconductor (CMOS) technology. PCM stores data by a thermal-induced phase transition between conductive polycrystalline (set) and resistive amorphous (reset) states in a thin film of chalcogenide material. The germanium antimony telluride alloy (GeSbTe or GST) used herein is one of the most commonly used chalcogenide-based phase change materials with a reversible phase change phenomenon [10, 11]. The switching is induced by Joule heating due to current flow. Therefore, the determination of the maximum temperature of the GST material is crucial in the PCM technology. In operation of the PCM device, a low required programming current and high resistance contrast between conductive polycrystalline (set) and resistive amorphous (reset) states are desired. A low required programming current indicates a low required power to operate the PCM devices. Device resistance fluctuation may disturb successful switching operations and leads to limited device cycle ability, and thus a high resistance ratio is crucial for PCMs with more programming cycles [12, 13].

Several schemes have been proposed to reduce the programming current and increase the resistance ratio of PCMs, such as reduction of the contact area between the heating electrode and GST layer [14, 15], bottom electrode contact engineering [16], increase of GST resistivity by impurity doping [17] and current concentration by thermally confined structure [18], and replacing GST by other materials [19–21]. However, the impacts of GST geometry and bottom electrode contact on PCM operation are still not clear. Therefore, this study investigates the dynamic thermal distribution of cylindrical PCMs by a three-dimensional (3D) electro-thermal time-domain simulation.

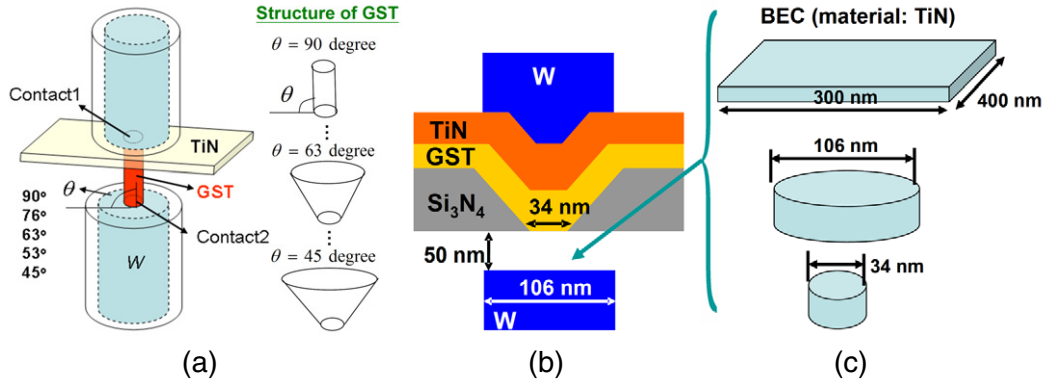

Figure 1. (a) The explored cylindrical PCM structure, whose cone angle of the GST alloy ranges from 90° to 45°. The bottom electrode contact (BEC) is inserted between the GST layer and the W, where the material of BEC is TiN, to improve the operation of the PCMs ((b) and (c)). The dimensions of the rectangular BEC are 400 nm × 300 nm. The radius (r) of the cylindrical BEC is 53 and 17 nm.

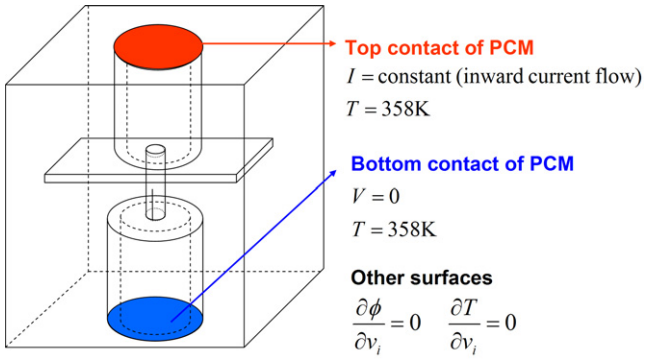

Figure 2. Boundary condition for the time-evolutionary electro-thermal simulation.

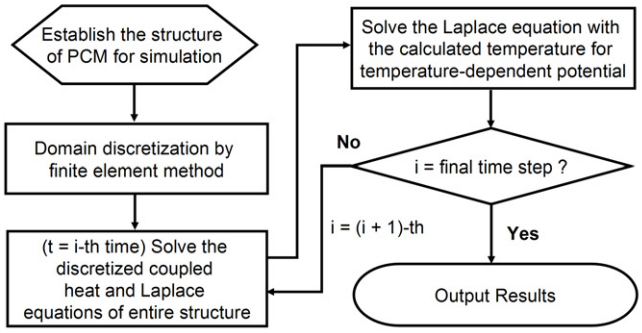

Figure 3. A flowchart for solving the coupled electro-thermal model to obtain the temperature and potential distribution of PCMs.

Figure 1 shows the simplified structure of PCM to study the effect of GST angle on PCM characteristics. The GST structure is a cone with different cone angles, ranging from 90° to 45°. The GST structure with a 90° GST cone angle exhibits the best operation performance of all. An experimentally validated cylindrical PCM with bottom electrode contact is then simulated to further reduce the impact of imperfect GST structure. Figures 1(b) and (c) show the cross-section of the explored PCMs. A bottom electrode contact (BEC) is inserted between the GST layer and the W, where the material of the BEC is TiN, to improve the operation of PCMs. The thickness of the BEC is fixed at 50 nm. The rectangular BEC has a 400 nm × 300 nm area; the cylindrical BECs have 53 and 17 nm radius (r). The required programming current is minimized at a cost of reducing the reset-to-set resistance ratio. The position of the BEC is thus shifted to examine the impact of reducing the contact area between the GST and BEC.

This paper is organized as follows. In section 2, we introduce the models to be solved and state the simulation flow for studying the operation characteristics of PCMs. In section 3, we examine the structure effects of the PCMs and propose an improvement approach. Finally, we draw conclusions and make suggestions for future work.

2. The electro-thermal simulation model

The temperature profile of the GST is estimated by the time-evolutionary electro-thermal simulation [2–4]. Table 1 shows the thermal and electrical parameters in the thermal simulation of PCM, in which the parameters are experimentally feasible. The computational model consists of a set of coupled Laplace and heat diffusion equations

$$\nabla(\sigma \cdot \nabla\phi) = 0, \tag{1}$$

$$\rho C_p \frac{\partial T}{\partial t} - K \cdot \nabla^2 T = \sigma |E|^2, \tag{2}$$

where T is temperature, t is time, σ is the electrical conductivity, ϕ is the electrical potential, E is electric field, and ρ is the density. K and C_p correspond to the thermal conductivity and the specific heat, respectively. Incorporating proper boundary conditions, as shown in the figure 2, finite element solution of these partial differential equations determines the potential and resulting temperature throughout the storage medium. Figure 3 illustrates the computational flowchart to solve the coupled electro-thermal model. First the explored structures are established for the 3D simulation, and apply the finite element method to do the domain discretization. Then the discretized coupled heat equation and Laplace equation for temperature and potential

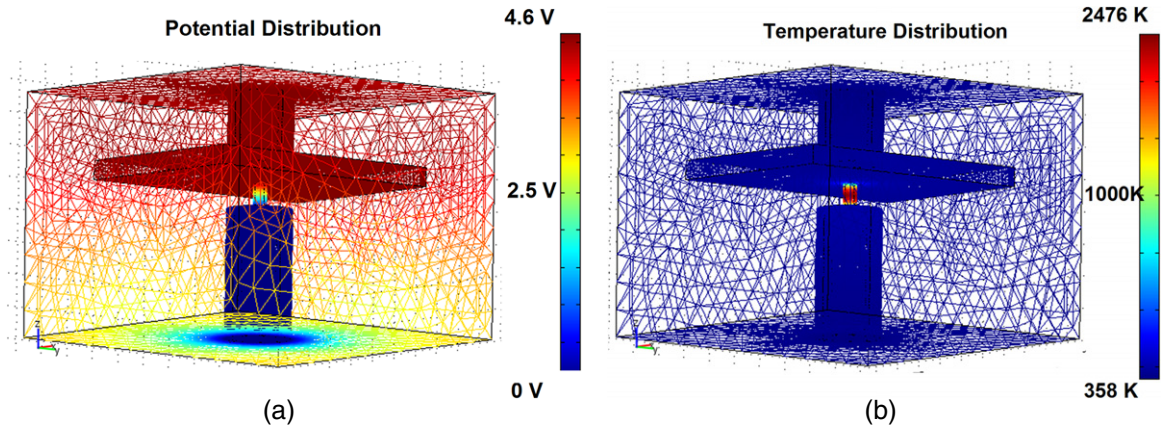

Figure 4. The (a) potential (b) and temperature distributions of the discretized PCMs with 90° GST cone angle, where a pulse current is input from the top of the PCM device and then flows through the entire device to ground.

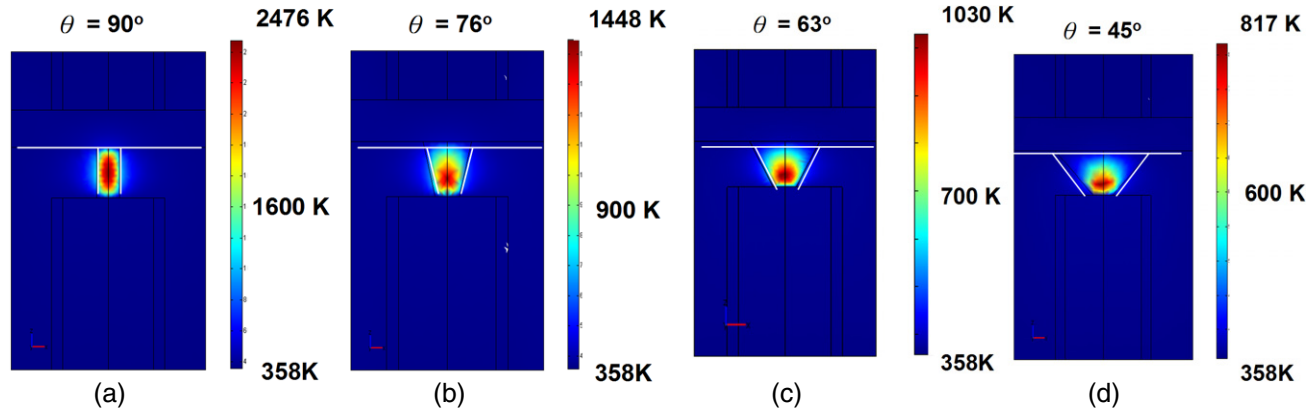

Figure 5. Temperature distribution of the cylindrical-shaped PCMs with (a) 90°, (b) 73°, (c) 63°, (d) and 45° GST cone angle, where the boundary temperature is 358 K.

Table 1. A list of the thermal and electrical parameters in the thermal simulation of PCM. We notice that the adopted parameters are experimentally feasible.

Material	Electric conductivity, σ ($1\ \Omega^{-1}\ m^{-1}$)	Thermal conductivity, K ($W\ K^{-1}\ m^{-1}$)	Specific heat, C_p ($J\ K^{-1}\ m^{-3}$)
GST ($T < 883$ K; crystalline)	6.03×10^4	0.4	1.25×10^6
GST($T \geqq 883$ K; amorphous)	3	0.2	1.25×10^6
TiN	4.54×10^5	10	0.7×10^6
W	7.107×10^6	174	2.55×10^6

distributions of the entire structure are solved at the ith time step. In the next step, the Laplace equation with the calculated temperature is solved for the temperature-dependent potential distribution at the ith time step. After that, we go back to solve the heat equation and Laplace equation for the next $(i + 1)$th time step. If the final time step is achieved, the results will be output.

3. Results and discussion

Figure 4(a) shows the potential distribution for the discretized cylindrical-shaped PCMs with 90° GST cone angle. A pulse current of 80 μA with 50 ns time duration is input from the top of the PCM device and then flows though the entire device to ground. The potential distribution varies most significantly in the GST alloy, and results in a large current density in the GST. Thus, the maximum temperature (hot spot) may occur inside the GST alloy, as plotted in figure 4(b), and induce the phase transition between conductive polycrystalline (set) and resistive amorphous (reset) states. A cross-sectional view of the temperature distribution is plotted in figure 5(a), where the hot spot temperature is 2476 K. Without losing generality, under the same programming current, the temperature distribution for PCMs with various GST cone angles, ranging from 76° to 45°, are studied in figures 5(b)–(d). The hot spot temperature is decreased with smaller cone angle and the position of the hot spot is shifted toward the bottom of the GST. The location of the hot spot

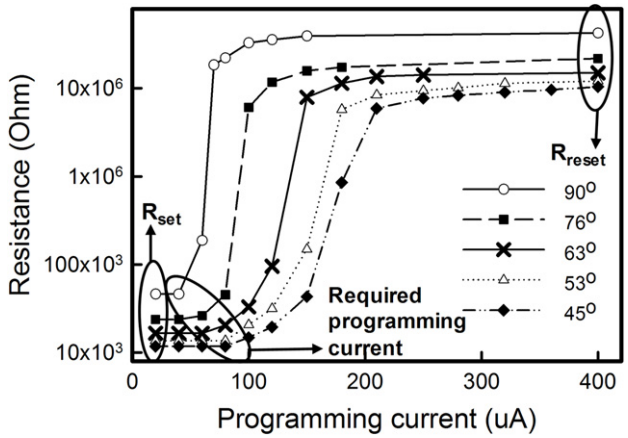

Figure 6. Resistance–programming current curves of the studied PCMs, in which the phase transition of PCMs from the conductive polycrystalline (set) state to the resistive amorphous (reset) state is examined. R_{set} and R_{reset} show the resistance of the set and reset states, and the required programming current (I_p) is defined as the starting point of the phase transition in the R–I curve.

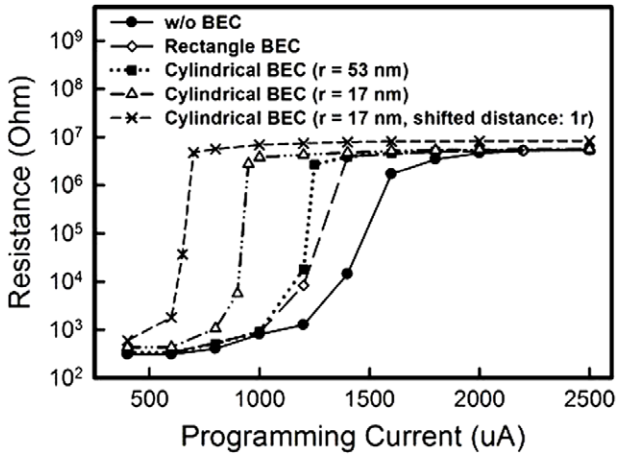

Figure 8. Resistance–programming current curves for the studied PCMs with and without BEC.

determines the initial position of the phase transition and the results show the different starting points of the phase transition in PCMs with different cone angles.

The phase transition of PCMs from the conductive polycrystalline (set) state to the resistive amorphous (reset) state is examined to study the geometrical variation influence on the operation of PCMs. The resistances of PCMs as a function of programming current are then studied in figure 6. The R_{set} and R_{reset} show the resistance of the set and reset state, and the required programming current (I_p) is defined as the starting point of the phase transition in the R–I curve. As shown in figure 6, the device with 90° GST cone angle has a lower required programming current than the others. Also, the steepest slope of the R–I curve during the set-to-reset transition is observed. The resistance of PCMs under various programming currents is explored in figure 7(a). As the programming current is increased, the resistance of the PCM is increased due to the increased portion of amorphous GST. The device with 90° GST cone angle also shows a large difference of resistance due to its smallest volume of GST. The large difference of resistance induces a fast transition of the R–I curve from the set state to the reset state, as shown in figure 6. The result also implies a larger resistance ratio of R_{reset}/R_{set} for PCMs with larger GST cone angle, as plotted in figure 7(b). The resistance ratio increases with increasing GST cone angle and then saturates as the GST cone angle becomes larger than 76°. The resistance ratio of the PCM with 63° GST cone angle is 90% of the PCM with 90° GST cone angle, the device with the largest resistance ratio. The result indicates that, to pursue a higher resistance contrast of the PCM, the manufacturability should be improved to provide a higher cone angle of PCMs. However, to compromise the manufacturability, the device with a cone angle larger than 63° is acceptable.

Due to the difficulty in achieving the vertical cone angle of GST, an approach is proposed to reduce the programming current and improve the resistance ratio by the aid of the bottom electrode contact (BEC) as shown in figure 1(c), where a 50 nm thickness TiN material is inserted between the GST

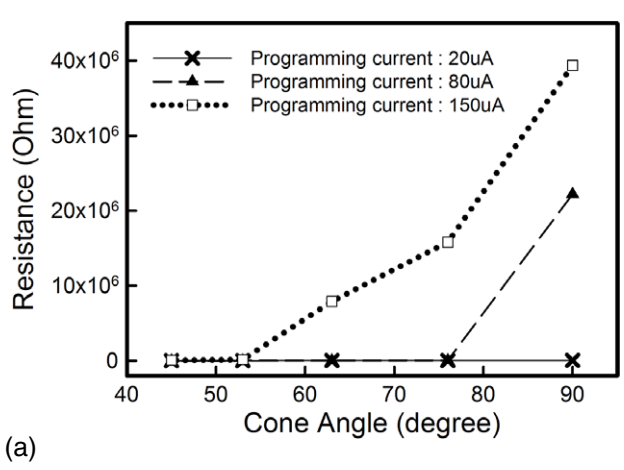

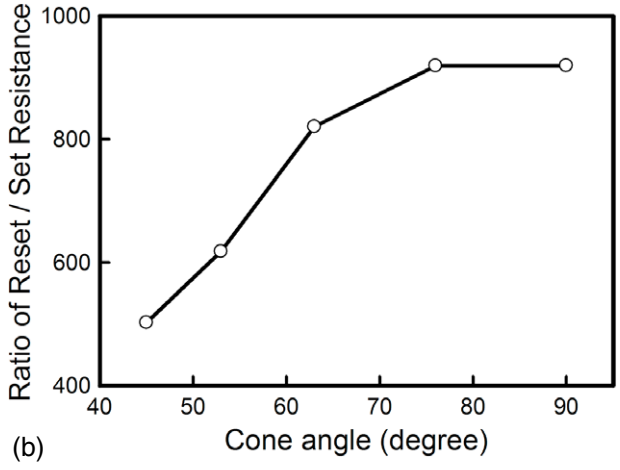

Figure 7. (a) The resistance and (b) the resistance ratio of PCMs as a function of GST cone angle.

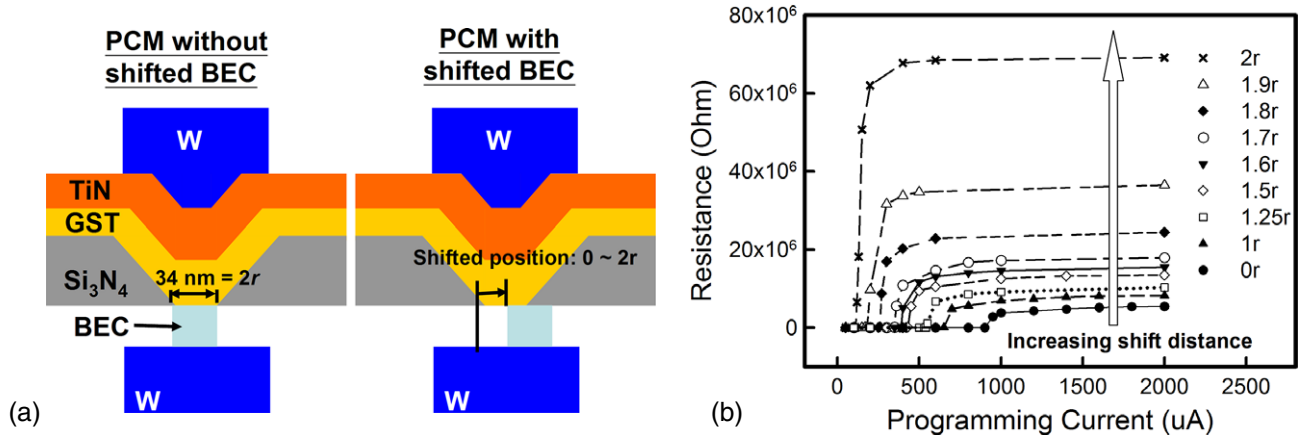

Figure 9. (a) Illustrations for PCMs with and without shifted BEC. (b) Resistance–programming current curves for the studied PCMs with shifted BEC, where the shift distance ranges from $1r$ to $2r$.

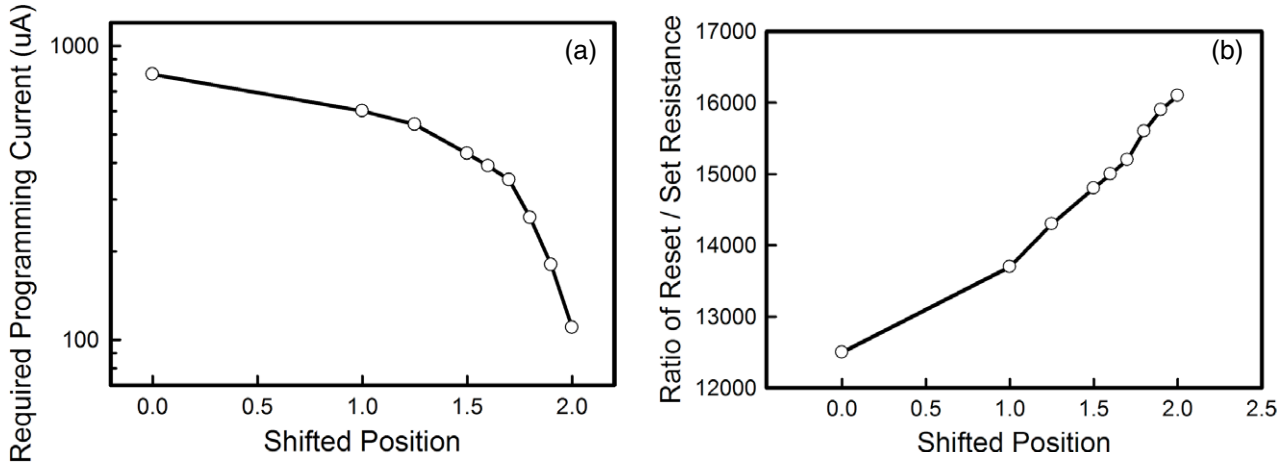

Figure 10. The (a) required programming current and (b) resistance ratio as a function of the shifted position of the BEC.

layer and the W. This study examines the rectangular BEC (400 nm × 300 nm) and the cylindrical BEC with 53 and 17 nm radius (r), as shown in figure 1(c). The cylindrical BEC with 17 nm radius is shifted to examine the impact of reducing the contact area between GST and BEC. The corresponding R–I characteristics are simulated in figure 8, where the results of the required programming current (I_p), reduction rate of I_p, and resistance ratio (R_{reset}/R_{set}) are summarized in table 2. The addition of BEC between the GST layer and W can effectively reduce the required programming current due to the increased resistance of the current flow path from the top of the PCM to ground. For the PCMs with rectangular BEC and 53 nm radius cylindrical BEC, the improvements are quite similar due to the same contact area between the GST layer and the BEC. The I_p of the cylindrical one is slightly better due to the smaller volume and thus higher resistance of the BEC. The I_p can be further reduced by using a cylindrical BEC with smaller radius. In this study, without losing generality, a cylindrical BEC with the same radius as the smallest radius of the GST layer (r = 17 nm) is examined. A 25% reduction of I_p is achieved. The result confirms the effectiveness of increasing the resistance of the PCM in reduction of the required programming current; however, the resistance ratio of the PCMs with BEC is reduced by 26% due to the increase of the set and reset resistance. Then, the position of the BEC is shifted to reduce the contact area between the GST layer and BEC. Without losing generality, we use the radius of the BEC as the unit of shifted distance of the BEC. The characteristics of the 17 nm radius PCM with shifted BEC (shifted distance: $1r$) are further simulated. It is interesting to find that I_p is reduced by 46%; moreover, the resistance ratio is higher than the original 17 nm radius PCM. The shift of the BEC seems to be effective in both reduction of I_p and increase of resistance ratio.

Figure 9(a) presents the PCMs with and without BEC displacement. The R–I characteristics of the shift distance ranging from $1r$ to $2r$ are studied in figure 9(b) to further explore the impact of the shifted BEC in PCMs. The displacement of the BEC can be achieved by shifting the mask in the formation process of the BEC. I_p is significantly reduced with increasing shift distance of the BEC. The reduction of the required programming current and the resistance ratio are plotted in figures 10(a) and (b), respectively. Comparing with the PCMs without BEC, I_p is reduced by a factor of 11, where the resistance ratio is only reduced by 6.9%. Although the

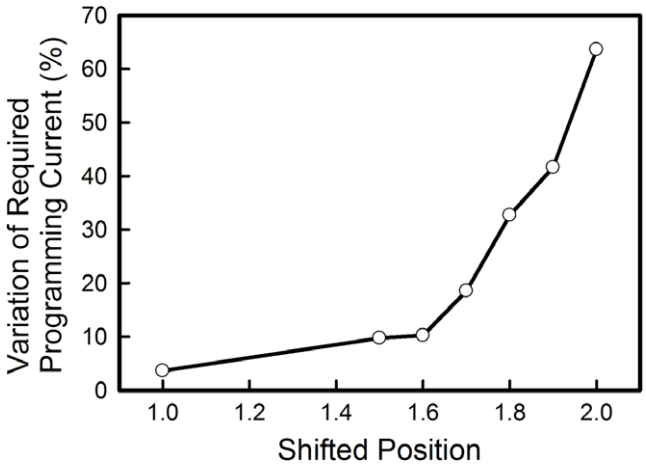

Figure 11. The variations of the required programming current as a function of the shifted position of the BEC, where a 10% variation of BEC position ($0.1r$) is introduced.

Table 2. Summarized operation characteristics for PCMs with and without BEC.

	I_p (μA)	I_p reduction[a]	R_{reset}/R_{set}
w/o BEC	1200	—	1.73×10^4
Rectangle BEC	1080	10%	1.63×10^4
Cylindrical BEC ($r = 53$ nm)	1020	15%	1.55×10^4
Cylindrical BEC ($r = 17$ nm)	900	25%	1.28×10^4
Cylindrical BEC ($r = 17$ nm, shifted distance: $1r = 17$ nm)	650	46%	1.37×10^4

[a] The I_p reduction is the difference of I_p normalized by the I_p of PCMs without BEC.

PCMs with large BEC shift can result in a lower required programming current and a higher reset/set resistance ratio, the stability of the required programming current is also an important issue in the fabrication of PCMs. For example, when a 10% variation of BEC position ($0.1r$) is introduced, the variation of I_p for the PCMs with $1r$-shifted BEC is about 20 μA; however, the variation for the PCMs with $2r$-shifted BEC is about 70 μA. The normalized variations for the $1r$-shifted BEC and $2r$-shifted BEC are 4% and 64%, respectively. Moreover, we notice that 50% of the PCMs with $2r$-shifted BEC may fail due to the separated BEC and GST layer. The variation of I_p as a function of BEC shift position is calculated in figure 11, where the I_p variation increases with increasing shift position of the BEC. The PCMs with a larger shift of BEC may become more sensitive to the process variation due to the larger variation of contact area between the GST layer and BEC. Therefore, to design PCMs with less than 10% I_p variation, PCMs with shifted BEC, where the shifted distance is equal to 1.5 times the BEC's radius, is worth considering.

4. Conclusions

In this study, a 3D electro-thermal time-domain simulation has been conducted for dynamic thermal analysis of the cylindrical-shaped PCMs. The effect of nanoscale GST alloy geometry on programming current and material phase transition has been investigated. The GST with an ideal 90° cone angle exhibits the lowest required programming current, the fastest phase transition characteristic, and the highest resistance ratio. Since the resistance ratio of the PCM with 63° GST cone angle is 90% of the PCM with 90° GST cone angle, the device with the largest resistance ratio, to compromise the manufacturability, the device with a cone angle larger than 63° cone angle is acceptable. The bottom electrode contact (BEC) is advanced to improve the operation of PCMs. For fixed contact area between the GST alloy and BEC, a 25% reduction of the required programming current is achieved by reducing the volume of the BEC. However, the resistance ratio is also reduced by 26%. Therefore, to further improve the performance of PCMs, the position of the BEC is shifted to reduce the contact area between the GST alloy and BEC. Comparing with the original PCMs without BEC, the required programming current is reduced by a factor of 11, where the resistance ratio is only decreased by 6.9%. However, we have to notice that the PCMs with a larger shift of BEC may become more sensitive to the process variation. Therefore, to design PCMs with less than 10% programming current variation, PCMs with shifted BEC, where the shifted distance is equal to 1.5 times the BEC's radius, is worth considering. This study quantitatively estimates the structure effect on the phase transition of the PCM and physically provides an insight into the design and technology of PCMs.

Acknowledgments

This work was supported by the Taiwan National Science Council (NSC) under contract NSC-97-2221-E-009-154-MY2 and contract NSC-96-2221-E-009-210, and by the Taiwan Semiconductor Manufacturing Company, Hsinchu, Taiwan, under a 2007–2009 grant.

References

[1] Anbarasu M and Asokan S 2007 The influence of network rigidity on the electrical switching behaviour of Ge–Te–Si glasses suitable for phase change memory applications *J. Phys. D: Appl. Phys.* **40** 7515–18

[2] Pirovano A, Lacaita A, Benvenuti A, Pellizzer F, Hudgens S and Bez R 2003 Scaling analysis of phase-change memory technology *IEEE Int. Electron Devices Mtg* pp 29.6.1–4

[3] Lai S and Lowrey T 2001 OUM—a 180 nm nonvolatile memory cell element technology for stand alone and embedded applications *Int. Electron Devices Mtg* pp 36.5.1–4

[4] Li Y, Yu S-M, Hwang C-H and Kuo Y-T 2008 Temperature dependence on the contact size of GeSbTe films for phase change memories *J. Comput. Electron.* **7** 138–41

[5] Ventrice D, Fantini P, Redaelli A, Pirovano A, Benvenuti A and Pellizzer F 2007 A phase change memory compact model for multilevel applications *IEEE Electron Device Lett.* **28** 973–5

[6] Kim Y-T, Hwang Y-N, Lee K-H, Lee S-H, Jeong C-W, Ahn S-J, Yeung F, Koh G-H and Jeong H-S 2005 Programming characteristics of phase change random access memory using phase change simulations *Japan. J. Appl. Phys.* **44** 2701–5

[7] Ovshinsky S R 1968 Reversible electrical switching phenomena in disordered structures *Phys. Rev. Lett.* **11** 1450
[8] Maimon J, Spall E, Quinn R and Schnur S 2001 Chalcogenide-based non-volatile memory technology *IEEE Proc. Aerospace Conf.* pp 2289–94
[9] Rao F, Song Z, Gong Y, Wu L, Feng S and Chen B 2008 Programming voltage reduction in phase change memory cells with tungsten trioxide bottom heating layer/electrode *Nanotechnology* **19** 445706
[10] Park S-J, Kim I-S, Kim S-K, Yoon S-M, Yu B-G and Choi S 2008 Phase transition characteristics and device performance of Si-doped $Ge_2Sb_2Te_5$ *Supercond. Sci. Technol.* **23** 105006
[11] Jeong J-H, Lee H S, Lee S, Lee T S, Kim W M, Zhe W, Kim S C, Oh K H and Cheong B-K 2009 Crystallization and memory programming characteristics of Ge-doped SbTe materials of varying Sb:Te ratio *J. Phys. D: Appl. Phys.* **42** 035104
[12] Zhong M, Song Z, Liu B, Wang L and Feng S 2008 Switching reliability improvement of phase change memory with nanoscale damascene structure by $Ge_2Sb_2Te_5$ CMP process *Electron. Lett.* **44** 322–23
[13] Pirovano A, Redaelli A, Pellizzer F, Ottogalli F, Tosi M, Ielmini D, Lacaita A and Bez R 2004 Reliability study of phase-change nonvolatile memories *IEEE Trans. Device Mater. Reliab.* **4** 422–7
[14] Hwang Y N *et al* 2003 Writing current reduction for high-density phase-change RAM *IEEE Int. Electron Devices Mtg* pp 37.1.1–4
[15] Ha Y H, Yi J H, Horii H, Park J H, Joo S H, Park S O, Chung U-I and Moon J T 2003 An edge contact type cell for phase change RAM featuring very low power consumption *Symp. on VLSI Technology* pp 175–6
[16] Wu L C, Song Z T, Rao F, Gong Y F, Liu B, Wang L Y, Liu W L and Feng S L 2008 Performance improvement of phase-change memory cell with cup-shaped bottom electrode contact *Appl. Phys. Lett.* 103107
[17] Horii H *et al* 2003 A novel cell technology using N-doped GeSbTe films for phase change RAM *Symp. on VLSI Technology* pp 177–8
[18] Karpov I V and Kostylev S A 2006 Set to reset programming in phase change memories *IEEE Electron Device Lett.* **27** 808–10
[19] Lankhorst M H R, Ketelaars B W S M M and Wolters R A M 2005 Low-cost and nanoscale non-volatile memory concept for future silicon chips *Nat. Mater.* **4** 347–52
[20] Rajesh R and Philip J 2003 Memory switching in In–Te glasses: results of heat-transport measurements *Supercond. Sci. Technol.* **18** 133–8
[21] Saheb P Z, Asokan S and Gowda K A 2003 Electrical switching studies of lead-doped germanium telluride glasses *Appl. Phys.* A **77** 665–8